processes

Article

Tungsten Oxide Modified V_2O_5-Sb_2O_3/TiO_2 Monolithic Catalyst: NH_3-SCR Activity and Sulfur Resistance

Liping Liu [1,2], Xiaodong Wu [2,*], Yue Ma [2], Jinyi Wang [1], Rui Ran [2], Zhichun Si [3] and Duan Weng [2]

[1] Huaneng Clean Energy Research Institute, Beijing 102209, China; lp_liu@qny.chng.com.cn (L.L.); jy_wang@qny.chng.com.cn (J.W.)
[2] School of Materials Science and Engineering, Tsinghua University, Beijing 100084, China; yue-ma16@mails.tsinghua.edu.cn (Y.M.); ranr@tsinghua.edu.cn (R.R.); duanweng@tsinghua.edu.cn (D.W.)
[3] Graduate School at Shenzhen, Tsinghua University, Shenzhen 518055, China; si.zhichun@sz.tsinghua.edu.cn
* Correspondence: wuxiaodong@tsinghua.edu.cn; Tel.: +86-158-1002-8863

Abstract: In this study, a V_2O_5-Sb_2O_3/TiO_2 monolithic catalyst was modified by introducing WO_3. The WO_3-modified catalyst exhibited enhanced catalytic activity in the measuring temperature range of 175–320 °C. The changes in dispersion of vanadia species were investigated by ultraviolet-visible (UV-Vis) spectroscopy and H_2 temperature-programmed reduction (H_2-TPR). A durability test was conducted in a wet SO_2-containing atmosphere at 220 °C for 25 h. The sulfate deposition was estimated by temperature-programmed decomposition (TPDC) of sulfates, thermo-gravimetric (TG) analysis, and temperature-programmed desorption (TPD) of NH_3. Isothermal SO_2 oxidation and temperature-programmed surface reaction (TPSR) of NH_4HSO_4 with NO were performed. Based on these characterizations, effects of WO_3 modification on the sulfate tolerance of the catalyst were explored.

Keywords: NH_3-SCR; vanadia species; tungsten oxide; low temperatures; sulfates

check for updates

Citation: Liu, L.; Wu, X.; Ma, Y.; Wang, J.; Ran, R.; Si, Z.; Weng, D. Tungsten Oxide Modified V_2O_5-Sb_2O_3/TiO_2 Monolithic Catalyst: NH_3-SCR Activity and Sulfur Resistance. *Processes* **2022**, *10*, 1333. https://doi.org/10.3390/pr10071333

Academic Editor: Zhenmeng Peng

Received: 21 May 2022
Accepted: 6 July 2022
Published: 8 July 2022

1. Introduction

Nitrogen oxides (NO_x) emitted from stationary and mobile sources cause many environmental pollution problems, including photochemical smog, ozone depletion, acid rain, and greenhouse effects [1–3]. Selective catalytic reduction (SCR) of NO_x with ammonia has been widely recognized as one of the most effective technologies for NO_x abatement [4–8]. V-based SCR catalysts have been widely commercially applied due to their high catalytic performance and good stability in the temperature region of 300–400 °C [9–11]. In stationary sources, to gain appropriate reaction temperature for catalysts, the SCR unit is commonly located upstream of the desulfurization and dust-removal facilities. However, high concentrations of SO_2 and ash in the exhaust gas may result in severe catalyst poisoning and shorten the service life of the catalyst in this case [12,13]. Alternatively, an SCR unit is located downstream of desulfurization and dust-removal units to prevent the catalyst from being exposed to high concentrations of SO_2 and ash, and to increase the recovery efficiency of waste heat [13,14]. It should be noted that uncaptured SO_2 still exists in the flue gas in this case, and the flue temperature is lowered to a temperature below 300 °C [15,16]. Thus, it is of significance to exploit the SCR catalyst with high NO_x conversion regarding low-temperature exhaust gas containing SO_2.

Metal oxide catalysts (e.g., Mn-, V-, Ce-based catalysts) have been widely investigated for their low-temperature NH_3-SCR activities, owing to their advantages of low cost and easy preparation [17–25]. Among these catalysts, V-based catalysts are considered a preferable choice for SO_2-containing flue gas purification at low temperatures, due to their superior sulfur resistance [26,27]. However, the NO_x conversions of V-based catalysts at low temperatures still need to be further improved to meet the increasingly stringent emission regulations. Over the past decades, several attempts to modify V-based catalysts have been reported. For instance, Zhang et al. [28] prepared F-doped V_2O_5/TiO_2 catalysts with improved NH_3-SCR activity at low temperatures, and they ascribed the enhanced activity to the fact that F-doping could improve the interaction of V_2O_5 with TiO_2 and facilitate the formation of reduced vanadia. Ma et al. [29] studied the effect of CeO_2 modification on the low-temperature NH_3-SCR activity of the V_2O_5-WO_3/TiO_2 catalyst. They demonstrated that V-O-Ce bridging bonds were formed in the catalyst, and the reducibility of the catalyst was enhanced due to the synergistic effect between Ce and V. The introduction of WO_3 can improve the NH_3-SCR activity of the catalyst by increasing the redox property and Brönsted acidity [30]. Indeed, Lietti et al. [31] observed that the V_2O_5-WO_3/TiO_2 catalyst has both higher transient and steady-state reactivity in SCR than the binary V_2O_5/TiO_2 counterpart. They reported the presence of a specific synergistic effect between V and W, which promoted the reoxidation of reduced vanadia [31]. Paganini et al. [32] also connected the superior redox properties of V_2O_5-WO_3/TiO_2 to the V–W electronic interaction. Chen et al. [27] reported that the introduction of tungsten benefits the generation of more low-valence vanadium species due to its promotional effect of capturing and transferring electrons, and thus the WO_3 modified catalyst exhibits superior low-temperature SCR activity to that of V_2O_5/TiO_2 catalyst after hydrothermal aging treatment. In contrast, Jaegers et al. attributed [33] the promotion effect of WO_3 to structural effects, including inducing the formation of oligomeric vanadia sites and generating adjacent surface sites rather than the electronic effect through in-situ spectroscopic measurements (i.e., MAS NMR, Raman and EPR). Conversely, the role of WO_3 as an acidity promoter is widely accepted. By combining experimental characterizations with DFT calculations, Sun et al. [34] studied the promotion effect of tungsten oxide on SCR activity of V_2O_5-$WO_3/Ti_{0.5}Sn_{0.5}O_2$ catalyst. They found that the number of the Brønsted acid sites increases with the loading amount of WO_3, resulting in higher SCR activity. Nuguid et al. [35] developed a characterization technique of modulated excitation Raman spectroscopy to access the mechanistic information that was currently unachievable with steady-state Raman experiments. They clarified that only a defined portion of VO_x species acted as catalytic active centers, which were coordinately unsaturated. Additionally, TiO_2 acted as an NH_3 reservoir and was indirectly involved in the SCR reaction.

The durability of low-temperature SCR catalysts in the presence of SO_2 also receives great attention. Kang et al. [36] constructed low-temperature SCR catalysts by mechanically mixing commercial V_2O_5-WO_3/TiO_2 with Fe_2O_3, and the obtained catalysts exhibited higher catalytic stability in the presence of SO_2 than V_2O_5-WO_3/TiO_2. They discovered that the formation of ammonium sulfates was hindered due to the production of iron sulfates from adjacent Fe_2O_3. Furthermore, iron sulfate could assist the NH_3-SCR reaction by supplying additional Brønsted acid sites. In recent years, antimony (Sb) has attracted increasing attention as an additive to promote the SCR performance of V-based catalysts [37]. Phil et al. [38,39] found that the Sb-doped V_2O_5/TiO_2 catalyst demonstrated not only higher NO_x conversions, but also better SO_2 resistance at low temperatures than catalysts containing other promoters (Pb, B, Cu, and P). It has been demonstrated in our previous work that the Sb-modified V_2O_5/TiO_2 catalyst indicated excellent deNO_x performance in the presence of SO_2 because the introduction of Sb_2O_3 can not only weaken the SO_2 oxidation activity, but also enhance the reactivity of NH_4HSO_4 with NO [40]. However, the low-temperature SCR activity of VSbTi monolithic catalyst must be further improved to meet increasingly stringent emission regulations [2].

This study aimed to introduce WO_3 to V_2O_5-Sb_2O_3/TiO_2 (VSbTi) catalyst to further improve catalytic performance at low temperatures. The VSbTi and W-modified monolithic catalysts were prepared by an extrusion-molding method. The effects of WO_3 addition on the surface properties, catalytic activity, and durability were clarified. Furthermore, the sulfur-poisoning mechanism of the modified catalyst was illustrated.

2. Experimental

2.1. Catalyst Preparation

VSbTi and VSbWTi cuboid monolithic catalysts were fabricated by an extrusion-molding method, using a vacuum mixing extruder (Zibo Shenyun Machinery, China, QLJ-150L). Firstly, the VSbTi catalyst (the mass ratio of V_2O_5:Sb_2O_3:TiO_2 = 2.7:2.0:95.3) was prepared by mixing mesoporous TiO_2 powders (Millennium Chemicals DT51, Baltimore, Maryland, USA, S_{BET} = 81 m^2/g) in an aqueous precursor solution containing 0.5 M antimony acetate (Sinopharm, Beijing, China, 97%) and 1.1 M ammonium metavanadate (Beijing Chemical Reagent, Beijing, China, 99.9%). After stirring for 2 h, the suspension was titrated with 20 wt.% ammonia hydroxide (Sinopharm Chemical Reagent, Beijing, China, GR) until the pH reached 10, and then stirred for another 6 h. Subsequently, the resulting precipitates were separated by filtration and desiccation. The additives of stearic acid, polyethylene oxide, and carboxymethyl cellulose were used to facilitate the extrusion process. The VSbTi monolithic catalyst was obtained through extrusion molding and calcination at 550 °C for 6 h. The size of the monolithic catalysts was 36 mm × 36 mm × 200 mm (length), and the size of the cubic channel was 6 mm × 6 mm. The VSbWTi monolithic catalyst (the mass ratio of V_2O_5:Sb_2O_3:WO_3:TiO_2 = 2.7:2.0:1.5:93.8) was prepared by the same method but with the addition of 0.1 M ammonium paratungstate (Sinopharm, Beijing, China, 99.5%) as a W precursor. The SO_2 resistance test was performed in a feed stream of 1000 ppm NO/1000 ppm NH_3/350 ppm SO_2/10% H_2O/N_2 at 220 °C for 25 h, and the corresponding sulfated catalysts after the durability test were denoted as VSbTi-S and VSbWTi-S, respectively.

2.2. Activity Measurement

Isothermal NH_3-SCR activity evaluation was conducted between 175 and 320 °C in a fixed-bed stainless-steel reactor. Both the stainless-steel reactor and monolithic catalysts were cuboid in shape. The monolithic catalyst was exposed to a feed stream of 1000 ppm NO/1000 ppm NH_3/350 ppm SO_2/5% O_2/10% H_2O/N_2 with a gas hourly space velocity of (GHSV) of 5000 h^{-1}. The effluent gases were monitored by a flue gas analyzer (ecom EN-2F, RBR, Germany) when the reaction reached equilibrium. The NO_x conversion was calculated according to the following equation:

$$NO_x \text{ conversion } (\%) = \frac{[NO]_{in} - [NO]_{out} - [NO_2]_{out}}{[NO]_{in}} \times 100 \quad (1)$$

To evaluate the activity of the catalysts for SO_2 oxidation, an isothermal reaction was performed in the same apparatus to that of SCR activity measurements with a feed stream consisting of 500 ppm SO_2, 5% O_2 and N_2 in balance (GHSV 50,000 h^{-1}). The produced SO_3 was absorbed by an aqueous solution containing 80 wt.% isopropyl alcohol. After reaction for 6 h, the obtained solution was titrated with 0.01 M $Ba(ClO_4)_2 \cdot 3H_2O$ using alizarin red S as an indicator. The SO_2 conversion was estimated according to the following equation:

$$SO_2 \text{ conversion } (\%) = \frac{[SO_3]_{out}}{[SO_2]_{in}} \times 100 \quad (2)$$

2.3. Characterizations

Considering the homogeneous property of monolithic catalysts prepared by extrusion molding, the catalyst powders were prepared for the following characterizations by crushing a middle fraction of monolithic catalysts and grinding the fraction in a mortar for 2 min. The crystallization structure of the catalysts was obtained by using an X-ray diffractometer (D8 Advance, Bruker, Germany) with a Cu Kα radiation (λ = 1.5418 Å), operating at an angle range of 20–80° and a scanning rate of 6 °/min.

The specific surface areas of the samples were measured using N_2 adsorption at −196 °C by the four-point Brunauer–Emmett–Teller (BET) method on an automatic surface analyzer (F-Sorb 3400, Gold APP Instrument). The catalysts were degassed at 200 °C for 2 h prior to the measurements.

Ultraviolet-visible (UV-vis) spectroscopy was conducted on a UV-2600 spectrophotometer (Shimadzu, Japan). $BaSO_4$ was used as a reference. The spectra were collected at room temperature (RT) in a wavelength region of 200–800 nm.

The temperature-programmed decomposition (TPDC) of sulfates deposited on the catalysts was performed in N_2 (50 mL/min) from RT to 750 °C at a heating rate of 10 °C/min. The released gases were monitored by a mass spectrometer (Omnistar 200, Germany).

The thermogravimetric (TG) measurement of the catalyst was performed on a Mettler Toledo TGA/DSC instrument from RT to 700 °C at a rate of 10 °C /min.

H_2 temperature-programmed reduction (H_2-TPR) was performed on a chemisorption analyzer (AutoChem II 2920, Micromeritics, USA) using a thermal conductivity detector (TCD). Prior to the test, 50 mg of samples were treated in O_2/N_2 (50 mL/min) at 200 °C for 30 min, then cooled down to RT. Only a low flow velocity was allowed for the chemisorption analyzer. To ensure sufficient contact between the samples and gaseous oxygen, a flow containing a high content of O_2/N_2 (20%) was employed for pretreatment before a H_2-TPR test. After purging in Ar (50 mL/min) for 20 min, the feed gas was changed into 10% H_2/Ar (50mL/min). Subsequently, the temperature was heated to 550 °C at a rate of 10 °C/min.

Temperature-programmed desorption of ammonia (NH_3-TPD) was performed on a Nicolet 380 FTIR gas analyzer (Thermo Fisher Scientific, Waltham, MA, USA). Prior to each test, the sample was pretreated in 5% O_2/N_2 (500 mL/min) at 200 °C for 30 min, then cooled down to 100 °C. Afterward, the sample was exposed to 1000 ppm NH_3/N_2 until saturation and then purged in N_2 to remove physically adsorbed NH_3. The adsorption saturation was recognized by the variation of NH_3 concentration less than 10 ppm around the inlet concentration within 10 min. The sample was heated to 500 °C at 10 °C /min in N_2 for NH_3 desorption.

3. Results

3.1. NH_3-SCR Activity

Figure 1a depicts the NH_3-SCR activities of VSbTi and VSbWTi monolithic catalysts. With the introduction of WO_3, the VSbWTi catalyst exhibits higher NO_x conversions at temperatures below 300 °C. The NO_x conversion reaches 90% at ca. 210 °C and 230 °C over VSbWTi and VSbTi, respectively. Because V-based catalysts produce little N_2O at low temperatures [41,42], the product from NO_x conversion is nearly 100% N_2 in the reaction. To measure the durability of the monolithic catalysts, a SO_2 resistance test was performed at 220 °C after the NH_3-SCR activity test, and the results are portrayed in Figure 1b. It is readily anticipated that the initial NO_x conversions in Figure 1b would be slightly lower than those in Figure 1a at the same temperature since the catalysts have been aged during the NH_3-SCR activity test. Compared with VSbTi, the VSbWTi catalyst deactivates more rapidly upon exposure to SO_2 and H_2O. After poisoning for 25 h, a drop of 12% in NO_x conversion occurs over VSbTi catalyst while VSbWTi exhibits a more evident decrease of 20%, so the poisoned catalysts indicate similar NO_x conversion (71–72%) at the end of the test. In real applications, the poisoned catalysts would undergo vapor washing and thermal regeneration when the NO_x conversion fell beneath a threshold value (e.g., 70%, depending on operation conditions). These results indicate that the introduction of WO_3 to VSbTi catalyst leads to higher deNO_x activity in the fresh state but lower sulfate tolerance.

3.2. Structural Properties

To understand the differences between VSbTi and VSbWTi in SO_2 resistance, crystalline structures of the fresh and sulfated catalysts were investigated. Characteristic diffraction peaks ascribed to anatase TiO_2 were observed in the XRD patterns of all the catalysts (Figure S1). No diffraction peaks assigned to vanadium oxide, tungsten oxide or antimony oxide were detected over all the catalysts, implying that these metal oxides exist in the forms of low crystallinity or well dispersion on the titania support. Diffraction features of crystalline sulfates were not observed on the sulfated catalyst.

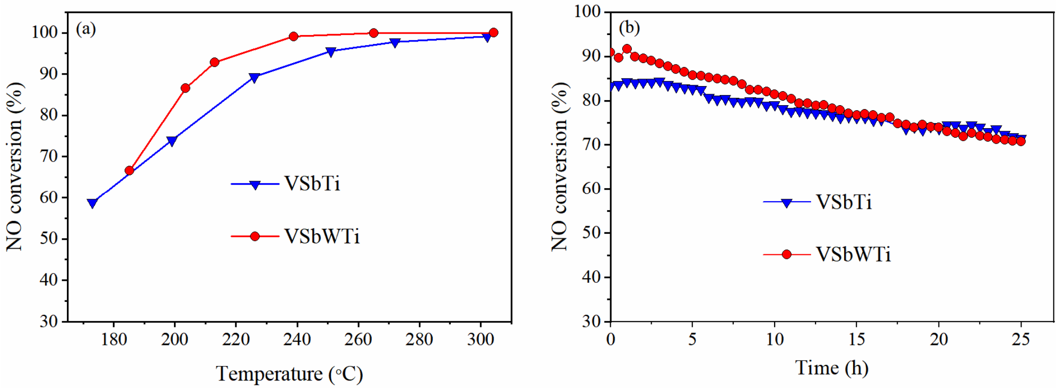

Figure 1. NO_x conversions of the monolithic catalysts: (**a**) NH_3-SCR activity; (**b**) durability test at 220 °C. Reaction conditions: NO = NH_3 = 1000 ppm, O_2 = 5%, H_2O = 10%, SO_2 = 350 ppm, N_2 in balance, and GHSV = 5000 h^{-1}.

The BET surface areas (S_{BET}) of VSbTi, VSbWTi, VSbTi-S, and VSbWTi-S are 37, 33, 30, and 27 m^2/g (Table S1), respectively. Compared with pure TiO_2 (DT51), a significant decrease in S_{BET} was found in all the catalysts, which is mainly associated with the introduction of impregnated metal oxides, including V_2O_5, Sb_2O_3, and WO_3. A similar phenomenon was also reported by Albonetti et al. [43], in which the S_{BET} of TiO_2 (DT51) decreases to 36 m^2/g after impregnation with 3 wt.% V_2O_5. As for the fresh catalysts, the introduction of WO_3 led to a further decrease in S_{BET}, which may be due to both the reduced content of TiO_2, and the pore blockage of the support by the added WO_3. As expected, the surface areas of sulfated catalysts decline, in comparison with the fresh counterparts, which can be explained by the pore-blocking effect of deposited sulfates [44]. In detail, the sulfur oxides react with ammonia and transform into ammonium sulfates, blocking the pores of the TiO_2 support [45,46].

UV-vis spectroscopy was adopted to identify the surface vanadium species in the fresh and sulfated catalysts. As indicated in Figure 2, the spectra are dominated by the absorption edge assigned to the $O^{2-} \rightarrow Ti^{4+}$ charge transfer (CT) transition of anatase TiO_2 at around 410 nm [21,47]. The broad absorption edge in the visible region of 450–550 nm is associated with the O-V CT transition of vanadium oxide, which is sensitive to the coordination structure of vanadia species [48,49], namely, the longer the adsorption edge wavelength representing the higher the coordination of polymeric vanadia species [49,50]. For the fresh catalysts, the adsorption edge position shifts from 534 to 542 nm after W modification. According to the literature [51], there is little contribution of WO_3 toward the absorption in the region of 400–550 nm with WO_3 addition lower than 7 wt.% in the TiO_2/SiO_2 catalyst. In our study, the loading of WO_3 is 1.5 wt.%, so the contribution of WO_3 to spectroscopic features could be ignored. Thus, it can be deduced that the introduction of WO_3 facilitates the redispersion of vanadia and results in the polymerization of vanadia species. Interestingly, the adsorption edge of the W-modified catalyst shifts significantly to a lower wavelength of 516 nm after sulfation, while the adsorption edge decreases slightly to 532 nm for VSbTi-S. This suggests that sulfation treatment leads to a more significant loss of polymeric vanadia species for the WO_3-modified catalyst. there is weak absorption at wavelengths higher than 600 nm for the fresh catalysts. This should be attributed to the presence of the highly polymerized vanadia species, which results in the band broadening and red-shift to a wavelength higher than 600 nm [52]. After sulfation, these highly polymerized vanadates disappear over VSbWTi-S and VSbTi-S since no absorption at the wavelength above 600 nm could be observed anymore. A similar phenomenon has also been discovered by Youn et al. [48].

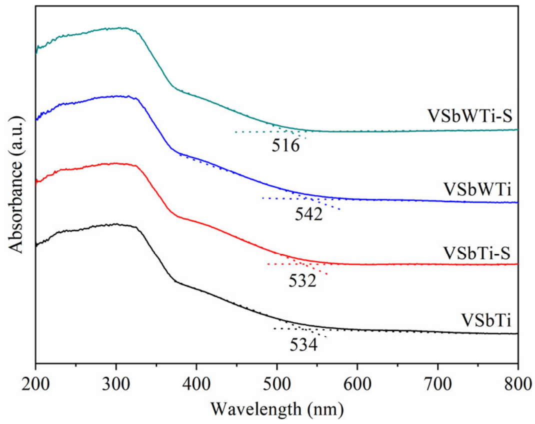

Figure 2. UV-vis spectra of the VSbTi, VsbWTi, VsbTi-S and VsbWTi-S catalysts.

To compare the sulfate deposition on the sulfated catalysts, the outlet gases (i.e., SO_2, NH_3, H_2O, and O_2) during the temperature-programmed decomposition process were analyzed by MS, and the results are provided in Figure 3. The releases of H_2O, O_2, and NH_3 at temperatures below 230 °C are attributed to the water, NH_3, and other surface-adsorbed impurities (e.g., hydroxyl and carbonate groups originated from the decomposition of additives during the calcination process) adsorbed on the catalysts [53]. In the temperature range of 230–370 °C, NH_3 release is observed, which is attributed to the decomposition of $(NH_4)_2SO_4$ to NH_4HSO_4 and NH_3 [20,54,55]. Subsequently, NH_4HSO_4 decomposes into NH_3, SO_2, O_2, and H_2O at higher temperatures (370–530 °C). It has been reported that the decomposition of metal sulfates occurs at higher temperatures than ammonium sulfates [56,57]. Clearly, a much larger amount of NH_3, SO_2, O_2, and H_2O are released from VSbWTi-S in the range of 230–710 °C (Figure 3b). This indicates that larger amounts of ammonium sulfates and metal sulfates deposit on the W-modified catalyst during sulfation. The bimodal feature of the SO_2 signal in the range of 330–460 °C is likely related to the decomposition of ammonium bisulfates bonded to different metal sites [58,59]. It is noted that the O and SO_2 signals do not follow the same profile. In Figure 3b, the SO_2 signal indicates a high contribution at around 400 °C and a smaller one close to 600 °C. When observing the O signal, the case is the opposite, with a low contribution at around 400 °C and a large contribution above 600 °C. The disappeared O signal at around 400 °C can be explained by NH_3 oxidation. It may be observed that the release window of NH_3 overlaps with those of SO_2 and O_2 at temperatures of about 400 °C due to the decomposition of ammonium sulfates. Part of the released O_2 is consumed with the catalytic oxidation of NH_3, resulting in a reduced O signal. At temperatures above 600 °C, the decomposition of metal sulfates does not produce NH_3, and the released O_2 is well maintained. Based on previous studies [36,54,60,61] and our work, the scheme of the formation and decomposition of AS and ABS is summarized in Figure S2.

The sulfates deposit on the catalysts were quantified by TG and the profiles are portrayed in Figure 4. The weight loss data are summarized in Table 1. Fresh catalysts only indicate one significant weight loss stage (Stage I), which is associated with the desorption of surface-adsorbed H_2O. Aside from this, sulfated catalysts display two other typical weight loss features (Stages II and III), and their weight losses in Stage I are larger than those of fresh counterparts due to H_2O and NH_3 adsorption during the sulfation treatment. Combining the MS results with the previous studies [40,62], the weight loss in Stage II should be assigned to the decomposition of ammonium sulfates, and that in Stage III can be ascribed to the decomposition of metal (i.e., V, Sb, Ti and W) sulfates. As listed in Table 1, the amount of ammonium sulfates and metal sulfates deposited on VSbWTi-S is about 9 and 3 times of that on VSbTi-S, respectively. This implies that WO_3 modification significantly accelerates the sulfate deposition on the catalyst, in accordance with the MS results.

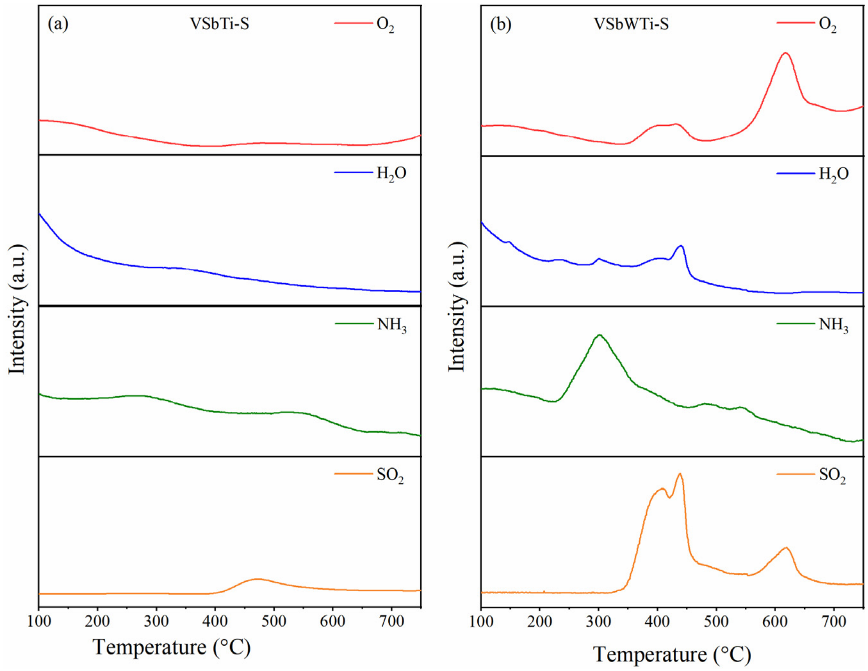

Figure 3. Gaseous products during the temperature-programmed decomposition of (**a**) VSbTi-S and (**b**) VsbWTi-S catalysts.

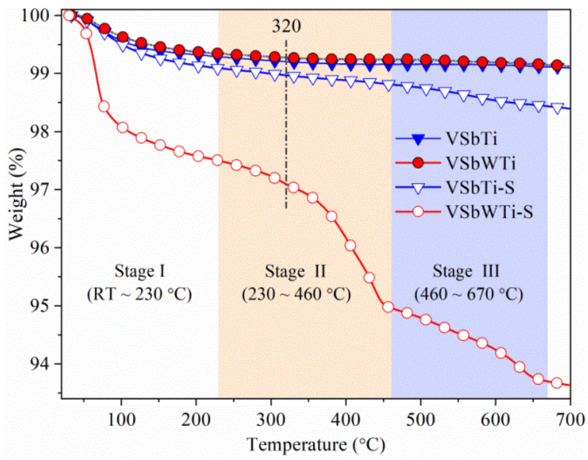

Figure 4. TG profiles of the VSbTi, VSbWTi, VSbTi-S, and VSbWTi-S catalysts.

Table 1. Weight loss of sulfated catalysts derived from the TG results.

Catalyst	Weight Loss (%)	
	Stage II (230–460 °C)	Stage III (460–670 °C)
VSbTi-S	0.28	0.38
VSbWTi-S	2.54	1.27

3.3. Surface Properties

To evaluate the redox properties of the fresh and sulfated catalysts, H_2-TPR tests were performed and the results are illustrated in Figure 5. Both fresh catalysts indicate one major reduction peak between 350 to 500 °C, assigned to the reduction from V^{5+} to V^{3+} [48,63]. This peak shifts towards higher temperatures with nearly unchanged H_2 consumption after WO_3 modification, which is attributed to the transformation of monomeric VO_x to polymeric VO_x species [48,64], in line with the UV-vis results (Figure 2). As for VSbWTi-S, a typical bimodal reduction characteristic is observed. The sharp peak centered at 448 °C arises from the reduction of sulfates, and the shoulder at 418 °C is assigned to the reduction of vanadia. Additionally, its total H_2 consumption (634 µmol/g) is much larger than the fresh counterpart due to the contribution of sulfate reduction. VSbTi-S indicates a similar bimodal reduction curve but with much smaller H_2 consumption (317 µmol/g). These results verify that much more sulfates deposit on the W-modified catalyst during sulfation. The low-temperature reduction peak shifts toward lower temperature after sulfation, and the temperature drop for VSbWTi-S (21 °C) is much larger than that of VSbTi-S (4 °C), demonstrating a more severe loss of polymeric vanadia species for the former catalyst. It should be noted that some gases other than H_2 can also contribute to the TCD response and interfere with the TPR profiles, which would cause some disturbance to the above H_2 consumption analysis.

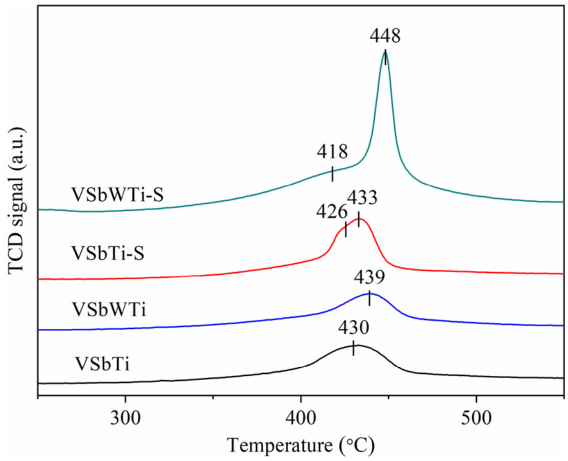

Figure 5. H_2-TPR curves of the VSbTi, VSbWTi, VSbTi-S, and VSbWTi-S catalysts.

Figure 6 portrays the NH_3-TPD curves of the catalysts. Both fresh catalysts exhibit similar desorption curves, illustrating that the introduced WO_3 has little effect on the surface acidity of the catalyst. After sulfation, the amount of total NH_3 desorption increases by 36% for VSbTi-S and 223% for VSbWTi-S. This can be explained primarily by the deposited sulfates that can also serve as acid sites [65,66]. Additionally, the decomposition of ammonium sulfates deposited on the catalyst surface contributes to NH_3 production during NH_3-TPD measurement, as clarified by MS analysis (Figure 3). The significantly increased NH_3 desorption of VSbWTi-S consolidates that W modification has a detrimental impact on the SO_2 resistance of VSbWTi catalyst that much more sulfates deposit on the W-modified catalyst upon sulfation.

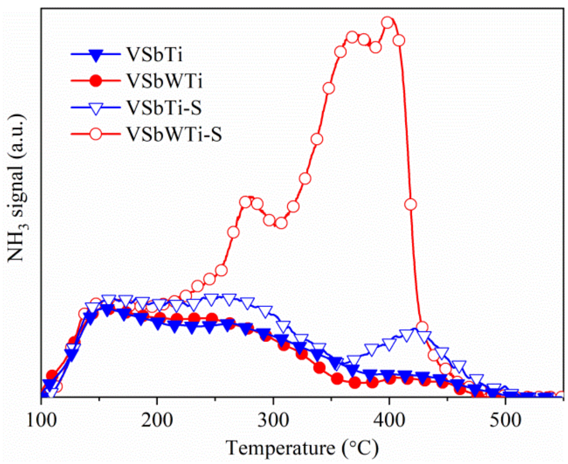

Figure 6. NH_3-TPD profiles of the VSbTi, VSbWTi, VSbTi-S, and VSbWTi-S catalysts.

3.4. Reactivity of Ammonium Bisulfate with NO

The sulfate generation on the catalyst is closely associated with the catalytic oxidation of SO_2. Thus, the SO_2 oxidation activity of fresh catalysts was measured, and the results are illustrated in Figure S3. Compared with VSbTi, VSbWTi exhibits a stronger ability to oxidize SO_2 to SO_3. As the first step of sulfate deposition, it is consistent with the result that abundant sulfates deposit on VSbWTi-S. NH_4HSO_4 (ABS) is generally the primary type of ammonium sulfate at low temperatures. Its accumulation on the catalyst depends on not only the generation of this salt, but also its decomposition via reaction with NO and O_2 to produce N_2, H_2O, and SO_2 [20].

Figure 7 indicates the TPSR profiles of the fresh catalysts impregnated with ABS in a NO + O_2 atmosphere without NH_3. In this case, ABS becomes the only source of ammonia for SCR reactions, and the variations of NO_x conversion reflect the reactivity of deposited NH_4HSO_4 with NO over different catalysts. Two NO_x conversion peaks occur at 195–200 °C and 370–400 °C, corresponding to the reaction of NO with NH_4^+ in NH_4HSO_4 and that with NH_3 coming from NH_4HSO_4 decomposition, respectively [60]. The low-temperature peak appears similar for the two catalysts, while the high-temperature peak is significantly retarded to a higher temperature (400 °C) over ABS/VSbWTi. These results indicate that the WO_3 modification not only promotes the generation of sulfates by enhanced catalytic oxidation of SO_2 to SO_3, but also weakens the decomposition of ammonium bisulfate with lower reactivity of ABS with NO. As a result, more severe deposition of ammonium sulfate species takes place on VSbWTi-S. Similarly, phenomena of more metal sulfate deposition may exist over this catalyst.

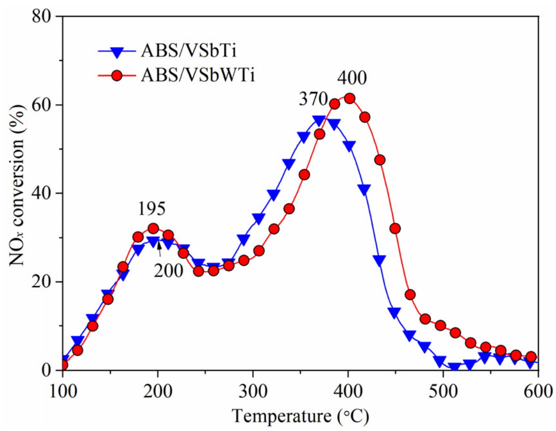

Figure 7. TPSR profiles of NH_4HSO_4 with NO over the catalysts impregnated with ABS. Reaction conditions: NO = 1000 ppm, O_2 = 5%, N_2 in balance and GHSV = 100,000 h^{-1}.

4. Discussion

It has been demonstrated in our previous work that Sb_2O_3-modified V_2O_5/TiO_2 catalyst (denoted as VSbTi) exhibited excellent deNO_x performance in the presence of SO_2 because the introduction of Sb_2O_3 can not only weaken the SO_2 oxidation, but also enhance the reactivity of NH_4HSO_4 with NO [40]. In this work, WO_3 is further introduced into VSbTi monolithic catalyst for improving the low-temperature SCR activity to meet increasingly stringent emission regulations (Figure 1a). The UV-vis and H_2-TPR results indicate that some monovanadates are transformed into polymeric vanadates in the WO_3 modified catalyst. It is well known that polymeric vanadate is more beneficial for NH_3-SCR reactions than monovanadate. These results suggest that the introduction of WO_3 in the VSbTi catalyst could change the dispersion of vanadia species and form more polymeric vanadates, which account for the enhanced NH_3-SCR activity of the VSbWTi catalyst. However, the durability of low-temperature SCR catalysts in the presence of SO_2 is always another important concern, and the WO_3 modification results in more severe deactivation in durability tests with SO_2 (Figure 1b). It has been discovered that more ammonium sulfates and metal sulfates deposit on the W-modified catalyst as confirmed by the UV-vis (Figure 2), MS-TPD (Figure 3), TG (Figure 4), H_2-TPR (Figure 5), and NH_3-TPD results (Figure 6). Moreover, the UV-vis and H_2-TPR results demonstrate more losses of polymeric vanadates over VSbWTi-S compared with VSbTi-S. The serious physical coverage of active sites by sulfates and the transformation of polymeric vanadates to metal sulfates are responsible for the more serious deactivation of the WO_3-modified catalyst upon sulfur attacking from the reaction atmosphere.

To further elucidate the different sulfur tolerances of the catalysts, SO_2 oxidation test and TPSR test with ABS were employed. Compared with VSbTi, higher catalytic oxidation of SO_2 to SO_3 is achieved over the W-modified catalyst (Figure S3). As indicated in Figure S2, this reaction is the initial step of the formation of sulfates on the catalyst during NH_3-SCR reactions. The generated SO_3 reacts with both NH_3 and catalyst components to deposit AS/ABS and metallic sulfates, respectively. These sulfates not only block the pore of catalysts (Table S1), but also reduce the availability of vanadate active sites [67–69]. The deposition of sulfates depends on the competition between the formation of sulfates and their consumption. The latter factor can be evaluated by the catalytic reaction of ABS (as a representative of deposited sulfates) with NO. The TPSR test (Figure 7) illustrates that the introduction of WO_3 hinders the consumption of impregnated ABS with NO, which is in line with the result that WO_3 modified catalyst displayed low sulfur resistance [70]. In this way, much more ammonium sulfates and metal sulfates are deposited over the VSbWTi catalyst upon sulfur exposure. The modification of WO_3 promotes the NH_3-SCR activity at low temperatures (<300 °C) but lowers sulfur resistance. These results are expected to give inspiration for designing strategies to gain satisfying low-temperature SCR catalysts under different application scenarios.

5. Conclusions

In this work, VSbTi and VSbWTi monolithic catalysts were prepared by an extrusion-molding method. WO_3 modification is found to promote the low-temperature (<320 °C) NH_3-SCR activity of V_2O_5-Sb_2O_3/TiO_2 catalyst, but weaken its sulfur resistance at 220 °C. On the one hand, WO_3 modification changes the dispersion of vanadia species to form more polymeric vanadates, which are more active sites than monomeric vanadates. On the other hand, the introduction of WO_3 leads to enhanced SO_2 oxidation ability and retarded reactivity of deposited NH_4HSO_4 with NO. As a result, more ammonium sulfates and metal sulfates deposit on the WO_3-modified catalyst during the durability test in the presence of SO_2 and H_2O, and lower sulfur resistance was discovered for this catalyst.

Supplementary Materials: The following supporting information can be downloaded at: https://www.mdpi.com/article/10.3390/pr10071333/s1, Figure S1: XRD patterns of the catalysts; Figure S2: Scheme of formation and decomposition of AS and ABS; Figure S3: SO_2 oxidation curves of the catalysts. Reaction conditions: SO_2 = 500 ppm, O_2 = 5%, N_2 in balance, and GHSV = 50,000 h^{-1}; Table S1: BET surface areas of catalysts.

Author Contributions: Experimental preparation and operation, writing—original draft, and employment of software, L.L. and Y.M.; writing—review and editing, X.W. and J.W.; supervision, R.R. and Z.S.; funding acquisition, D.W. All authors have read and agreed to the published version of the manuscript.

Funding: The authors gratefully acknowledge financial support from the National Key Research and Development Program of China (No. 2017YFC0211202).

Conflicts of Interest: The authors declare no conflict of interest.

References

1. Liu, F.; Yu, Y.; He, H. Environmentally-benign catalysts for the selective catalytic reduction of NO_x from diesel engines: Structure–activity relationship and reaction mechanism aspects. *Chem. Commun.* **2014**, *50*, 8445–8463. [CrossRef]
2. Chen, C.; Cao, Y.; Liu, S.; Chen, J.; Jia, W. Review on the latest developments in modified vanadium-titanium-based SCR catalysts. *Chin. J. Catal.* **2018**, *39*, 1347–1365. [CrossRef]

3. Yu, S.; Zhang, J. Numerical Investigation on the Intraphase and Interphase Mass Transfer Limitations for NH_3-SCR over Cu-ZSM-5. *Processes* **2021**, *9*, 1966. [CrossRef]
4. Han, L.; Cai, S.; Gao, M.; Hasegawa, J.-Y.; Wang, P.; Zhang, J.; Shi, L.; Zhang, D. Selective Catalytic Reduction of NO_x with NH_3 by Using Novel Catalysts: State of the Art and Future Prospects. *Chem. Rev.* **2019**, *119*, 10916–10976. [CrossRef]
5. Lai, J.-K.; Wachs, I.E. A Perspective on the Selective Catalytic Reduction (SCR) of NO with NH_3 by Supported V_2O_5-WO_3/TiO_2 Catalysts. *ACS Catal.* **2018**, *8*, 6537–6551. [CrossRef]
6. Maitarad, P.; Meeprasert, J.; Shi, L.; Limtrakul, J.; Zhang, D.; Namuangruk, S. Mechanistic insight into the selective catalytic reduction of NO by NH3 over low-valent titanium-porphyrin: A DFT study. *Catal. Sci. Technol.* **2015**, *6*, 3878–3885. [CrossRef]
7. Song, J.; Wang, Z.; Cheng, X.; Wang, X. State-of-Art Review of NO Reduction Technologies by CO, CH_4 and H_2. *Processes* **2021**, *9*, 563. [CrossRef]
8. Mehdi, G.; Zhou, S.; Zhu, Y.; Shah, A.H.; Chand, K. Numerical Investigation of SCR Mixer Design Optimization for Improved Performance. *Processes* **2019**, *7*, 168. [CrossRef]
9. Xu, J.; Chen, G.; Guo, F.; Xie, J. Development of wide-temperature vanadium-based catalysts for selective catalytic reducing of NOx with ammonia: Review. *Chem. Eng. J.* **2018**, *353*, 507–518. [CrossRef]
10. Chang, H.; Li, J.; Su, W.; Shao, Y.; Hao, J. A novel mechanism for poisoning of metal oxide SCR catalysts: Base–acid explanation correlated with redox properties. *Chem. Commun.* **2014**, *50*, 10031–10034. [CrossRef]
11. Guo, M.; Lis, B.M.; Ford, M.E.; Wachs, I.E. Effect of redox promoters (CeOx and CuOx) and surface sulfates on the selective catalytic reduction (SCR) of NO with NH3 by supported V_2O_5-WO_3/TiO_2 catalysts. *Appl. Catal. B Environ.* **2022**, *306*, 121108. [CrossRef]
12. Zheng, Y.; Jensen, A.D.; Johnsson, J.E. Deactivation of V_2O_5-WO_3-TiO_2 SCR catalyst at a biomass-fired combined heat and power plant. *Appl. Catal. B Environ.* **2005**, *60*, 253–264. [CrossRef]
13. Xi, Y.; Ottinger, N.A.; Liu, Z.G. New insights into sulfur poisoning on a vanadia SCR catalyst under simulated diesel engine operating conditions. *Appl. Catal. B Environ.* **2014**, *160–161*, 1–9. [CrossRef]
14. Magnusson, M.; Fridell, E.; Härelind, H. Improved low-temperature activity for marine selective catalytic reduction systems. *Proc. Inst. Mech. Eng. Part M J. Eng. Marit. Environ.* **2014**, *230*, 126–135. [CrossRef]
15. Khatri, N.J.; Johnson, J.H.; Leddy, D.G. *The Characterization of the Hydrocarbon and Sulfate Fractions of Diesel Particulate Matter*; SAE Technical Paper 780111; SAE: Warrendale, PA, USA, 1978; pp. 469–492. [CrossRef]
16. Wall, J.C.; Hoekman, S.K. *Fuel Composition Effects on Heavy-Duty Diesel Particulate Emissions*; SAE Technical Paper 841364; SAE: Warrendale, PA, USA, 1984; pp. 1–42. [CrossRef]
17. Zhou, X.; Wang, P.; Shen, Z.; Chen, S.; Wang, Q.; Cheng, D.; Zhang, D. Low-temperature NOx reduction over hydrothermally stable SCR catalysts by engineering low-coordinated Mn active sites. *Chem. Eng. J.* **2022**, *442*, 136182. [CrossRef]
18. Xu, T.; Wang, C.; Wu, X.; Zhao, B.; Chen, Z.; Weng, D. Modification of MnCo2Ox catalysts by NbOx for low temperature selective catalytic reduction of NO with NH_3. *RSC Adv.* **2016**, *6*, 97004–97011. [CrossRef]
19. Zhou, J.; Guo, R.-T.; Zhang, X.-F.; Liu, Y.-Z.; Duan, C.-P.; Wu, G.-L.; Pan, W.-G. Cerium Oxide-Based Catalysts for Low-Temperature Selective Catalytic Reduction of NO_x with NH_3: A Review. *Energy Fuels* **2021**, *35*, 2981–2998. [CrossRef]
20. Ye, D.; Qu, R.; Song, H.; Gao, X.; Luo, Z.; Ni, M.; Cen, K. New insights into the various decomposition and reactivity behaviors of NH_4HSO_4 with NO on V_2O_5/TiO_2 catalyst surfaces. *Chem. Eng. J.* **2016**, *283*, 846–854. [CrossRef]
21. Arfaoui, J.; Ghorbel, A.; Petitto, C.; Delahay, G. Novel V_2O_5-CeO_2-TiO_2-SO_4^{2-} nanostructured aerogel catalyst for the low temperature selective catalytic reduction of NO by NH3 in excess O_2. *Appl. Catal. B Environ.* **2018**, *224*, 264–275. [CrossRef]
22. Purbia, R.; Choi, S.Y.; Kim, H.J.; Ye, B.; Jeong, B.; Lee, D.H.; Park, H.; Kim, H.-D.; Baik, J.M. Cu- and Ce-promoted nano-heterostructures on vanadate catalysts for low-temperature NH3–SCR activity with improved SO2 and water resistance. *Chem. Eng. J.* **2022**, *437*, 135427. [CrossRef]
23. Wang, B.; Yang, Q. Optimization of Roasting Parameters for Recovery of Vanadium and Tungsten from Spent SCR Catalyst with Composite Roasting. *Processes* **2021**, *9*, 1923. [CrossRef]
24. Cheng, K.; Liu, J.; Zhang, T.; Li, J.; Zhao, Z.; Wei, Y.; Jiang, G.; Duan, A. Effect of Ce doping of TiO_2 support on NH_3-SCR activity over V_2O_5-WO_3/CeO_2-TiO_2 catalyst. *J. Environ. Sci.* **2014**, *26*, 2106–2113. [CrossRef] [PubMed]
25. Liu, J.; Huo, Y.; Shi, X.; Liu, Z.; Shan, Y.; Yu, Y.; Shan, W.; He, H. Insight into the remarkable enhancement of NH_3-SCR performance of Ce-Sn oxide catalyst by tungsten modification. *Catal. Today* **2022**, *in press*. [CrossRef]
26. Shi, Y.; Tan, S.; Li, S.; Zhao, J.; Xia, Y.; Lv, B.; Li, W. Inhibitory effect of SO_2 on side reactions of NH_3-SCR over olivine. *Catal. Sci. Technol.* **2015**, *5*, 3613–3623. [CrossRef]
27. Chen, H.; Xia, Y.; Fang, R.; Huang, H.; Gan, Y.; Liang, C.; Zhang, J.; Zhang, W.; Liu, X. The effects of tungsten and hydrothermal aging in promoting NH_3-SCR activity on V_2O_5/WO_3-TiO_2 catalysts. *Appl. Surf. Sci.* **2018**, *459*, 639–646. [CrossRef]
28. Zhang, S.; Zhong, Q.; Zhao, W.; Li, Y. Surface characterization studies on F-doped V_2O_5/TiO_2 catalyst for NO reduction with NH_3 at low-temperature. *Chem. Eng. J.* **2014**, *253*, 207–216. [CrossRef]
29. Ma, Z.; Wu, X.; Feng, Y.; Si, Z.; Weng, D.; Shi, L. Low-temperature SCR activity and SO2 deactivation mechanism of Ce-modified V_2O_5-WO_3/TiO_2 catalyst. *Prog. Nat. Sci.* **2015**, *25*, 342–352. [CrossRef]
30. Arfaoui, J.; Ghorbel, A.; Petitto, C.; Delahay, G. New CeO_2-TiO_2, WO_3-TiO_2 and WO_3-CeO_2-TiO_2 mesoporous aerogel catalysts for the low temperature selective catalytic reduction of NO by NH_3. *J. Porous Mater.* **2021**, *28*, 1535–1543. [CrossRef]

31. Lietti, L.; Alemany, J.; Forzatti, P.; Busca, G.; Ramis, G.; Giamello, E.; Bregani, F. Reactivity of V_2O_5-WO_3/TiO_2 catalysts in the selective catalytic reduction of nitric oxide by ammonia. *Catal. Today* **1996**, *29*, 143–148. [CrossRef]
32. Paganini, M.C.; Dall'Acqua, L.; Giamello, E.; Lietti, L.; Forzatti, P.; Busca, G. An EPR Study of the Surface Chemistry of the V_2O_5-WO_3/TiO_2 Catalyst: Redox Behaviour and State of V(IV). *J. Catal.* **1997**, *166*, 195–205. [CrossRef]
33. Jaegers, N.R.; Lai, J.; He, Y.; Walter, E.; Dixon, D.A.; Vasiliu, M.; Chen, Y.; Wang, C.; Hu, M.Y.; Mueller, K.T.; et al. Mechanism by which Tungsten Oxide Promotes the Activity of Supported V_2O_5/TiO_2 Catalysts for NO_X Abatement: Structural Effects Revealed by ^{51} V MAS NMR Spectroscopy. *Angew. Chem. Int. Ed.* **2019**, *58*, 12609–12616. [CrossRef]
34. Sun, C.; Dong, L.; Yu, W.; Liu, L.; Li, H.; Gao, F.; Dong, L.; Chen, Y. Promotion effect of tungsten oxide on SCR of NO with NH3 for the V_2O_5-WO_3/$Ti_{0.5}Sn_{0.5}O_2$ catalyst: Experiments combined with DFT calculations. *J. Mol. Catal. A Chem.* **2011**, *346*, 29–38. [CrossRef]
35. Nuguid, R.J.G.; Ferri, D.; Marberger, A.; Nachtegaal, M.; Kröcher, O. Modulated Excitation Raman Spectroscopy of V_2O_5/TiO_2: Mechanistic Insights into the Selective Catalytic Reduction of NO with NH_3. *ACS Catal.* **2019**, *9*, 6814–6820. [CrossRef]
36. Kang, T.H.; Youn, S.; Kim, D.H. Improved catalytic performance and resistance to SO_2 over V_2O_5-WO_3/TiO_2 catalyst physically mixed with Fe_2O_3 for low-temperature NH_3-SCR. *Catal. Today* **2020**, *376*, 95–103. [CrossRef]
37. Xu, C.; Liu, J.; Zhao, Z.; Yu, F.; Cheng, K.; Wei, Y.; Duan, A.; Jiang, G. NH_3-SCR denitration catalyst performance over vanadium–titanium with the addition of Ce and Sb. *J. Environ. Sci.* **2015**, *31*, 74–80. [CrossRef] [PubMed]
38. Haheon, P.; Chungsoon, H.; Ohyoung, J. Selective catalytic NOx reduction on Antimony promoted V_2O_5-Sb/TiO_2 catalyst. *Rare Met.* **2006**, *25*, 84–88. [CrossRef]
39. Phil, H.H.; Reddy, M.P.; Kumar, P.A.; Ju, L.K.; Hyo, J.S. SO_2 resistant antimony promoted V_2O_5/TiO_2 catalyst for NH_3-SCR of NOx at low temperatures. *Appl. Catal. B Environ.* **2008**, *78*, 301–308. [CrossRef]
40. Xu, T.; Wu, X.; Gao, Y.; Lin, Q.; Hu, J.; Weng, D. Comparative study on sulfur poisoning of V_2O_5-Sb_2O_3/TiO_2 and V_2O_5-WO_3/TiO_2 monolithic catalysts for low-temperature NH_3-SCR. *Catal. Commun.* **2017**, *93*, 33–36. [CrossRef]
41. Kumar, P.A.; Jeong, Y.E.; Gautam, S.; Ha, H.P.; Lee, K.J.; Chae, K.H. XANES and DRIFTS study of sulfated Sb/V/Ce/TiO_2 catalysts for NH_3-SCR. *Chem. Eng. J.* **2015**, *275*, 142–151. [CrossRef]
42. Shen, M.; Li, C.; Wang, J.; Xu, L.; Wang, W.; Wang, J. New insight into the promotion effect of Cu doped V_2O_5/WO_3-TiO_2 for low temperature NH_3-SCR performance. *RSC Adv.* **2015**, *5*, 35155–35165. [CrossRef]
43. Albonetti, S.; Blasioli, S.; Bonelli, R.; Mengou, J.E.; Scirè, S.; Trifirò, F. The role of acidity in the decomposition of 1,2-dichlorobenzene over TiO_2-based V_2O_5/WO_3 catalysts. *Appl. Catal. A Gen.* **2008**, *341*, 18–25. [CrossRef]
44. Kubacka, A.; Iglesias-Juez, A.; di Michiel, M.; Becerro, A.I.; Fernández-García, M. Morphological and structural behavior of TiO_2 nanoparticles in the presence of WO_3: Crystallization of the oxide composite system. *Phys. Chem. Chem. Phys.* **2014**, *16*, 19540–19549. [CrossRef]
45. Maqbool, M.S.; Pullur, A.K.; Ha, H.P. Novel sulfation effect on low-temperature activity enhancement of CeO_2-added Sb-V_2O_5/TiO_2 catalyst for NH_3-SCR. *Appl. Catal. B Environ.* **2014**, *152–153*, 28–37. [CrossRef]
46. Kwon, D.W.; Park, K.H.; Hong, S.C. Enhancement of SCR activity and SO_2 resistance on VOx/TiO_2 catalyst by addition of molybdenum. *Chem. Eng. J.* **2016**, *284*, 315–324. [CrossRef]
47. Tang, F.; Xu, B.; Shi, H.; Qiu, J.; Fan, Y. The poisoning effect of Na+ and Ca2+ ions doped on the V_2O_5/TiO_2 catalysts for selective catalytic reduction of NO by NH_3. *Appl. Catal. B Environ.* **2010**, *94*, 71–76. [CrossRef]
48. Youn, S.; Jeong, S.; Kim, D.H. Effect of oxidation states of vanadium precursor solution in V_2O_5/TiO_2 catalysts for low temperature NH3 selective catalytic reduction. *Catal. Today* **2014**, *232*, 185–191. [CrossRef]
49. Xu, Y.; Wu, X.; Lin, Q.; Hu, J.; Ran, R.; Weng, D. SO_2 promoted V_2O_5-MoO_3/TiO_2 catalyst for NH_3-SCR of NO at low temperatures. *Appl. Catal. A Gen.* **2018**, *570*, 42–50. [CrossRef]
50. Xu, Y.; Wu, X.; Cao, L.; Ma, Y.; Ran, R.; Si, Z.; Weng, D.; Ma, Z.; Wang, B. Crystal orientation-dependent activity of tungsten-based catalysts for selective catalytic reduction of NO with NH_3. *J. Catal.* **2019**, *375*, 294–303. [CrossRef]
51. Yanyan, L.; Kurniawan, T.A.; Ying, Z.; Albadarin, A.B.; Walker, G. Enhanced photocatalytic degradation of acetaminophen from wastewater using WO_3/TiO_2/SiO_2 composite under UV–VIS irradiation. *J. Mol. Liq.* **2017**, *243*, 761–770. [CrossRef]
52. Srinivas, D.; Hölderich, W.; Kujath, S.; Valkenberg, M.; Raja, T.; Saikia, L.; Hinze, R.; Ramaswamy, V. Active sites in vanadia/titania catalysts for selective aerial oxidation of β-picoline to nicotinic acid. *J. Catal.* **2008**, *259*, 165–173. [CrossRef]
53. Song, L.; Chao, J.; Fang, Y.; He, H.; Li, J.; Qiu, W.; Zhang, G. Promotion of ceria for decomposition of ammonia bisulfate over V_2O_5-MoO_3/TiO_2 catalyst for selective catalytic reduction. *Chem. Eng. J.* **2016**, *303*, 275–281. [CrossRef]
54. Shi, Y.-J.; Shu, H.; Zhang, Y.-H.; Fan, H.-M.; Zhang, Y.-P.; Yang, L.-J. Formation and decomposition of NH_4HSO_4 during selective catalytic reduction of NO with NH_3 over V_2O_5-WO_3/TiO_2 catalysts. *Fuel Process. Technol.* **2016**, *150*, 141–147. [CrossRef]
55. Ye, D.; Qu, R.; Song, H.; Zheng, C.; Gao, X.; Luo, Z.; Ni, M.; Cen, K. Investigation of the promotion effect of WO_3 on the decomposition and reactivity of NH_4HSO_4 with NO on V_2O_5-WO_3/TiO_2 SCR catalysts. *RSC Adv.* **2016**, *6*, 55584–55592. [CrossRef]
56. Jangjou, Y.; Do, Q.; Gu, Y.; Lim, L.-G.; Sun, H.; Wang, D.; Kumar, A.; Li, J.; Grabow, L.C.; Epling, W.S. Nature of Cu Active Centers in Cu-SSZ-13 and Their Responses to SO_2 Exposure. *ACS Catal.* **2018**, *8*, 1325–1337. [CrossRef]
57. Liang, Q.; Li, J.; He, H.; Yue, T.; Tong, L. Effects of SO_2 and H_2O on low-temperature NO conversion over F-V_2O_5-WO_3/TiO_2 catalysts. *J. Environ. Sci.* **2019**, *90*, 253–261. [CrossRef] [PubMed]
58. Tagawa, H. Thermal decomposition temperatures of metal sulfates. *Thermochim. Acta* **1984**, *80*, 23–33. [CrossRef]

59. Han, L.; Gao, M.; Hasegawa, J.-Y.; Li, S.; Shen, Y.; Li, H.; Shi, L.; Zhang, D. SO_2-Tolerant Selective Catalytic Reduction of NO_x over Meso-TiO_2@Fe_2O_3@Al_2O_3 Metal-Based Monolith Catalysts. *Environ. Sci. Technol.* **2019**, *53*, 6462–6473. [CrossRef]
60. Ye, D.; Qu, R.; Zheng, C.; Cen, K.; Gao, X. Mechanistic investigation of enhanced reactivity of NH_4HSO_4 and NO on Nb- and Sb-doped VW/Ti SCR catalysts. *Appl. Catal. A Gen.* **2018**, *549*, 310–319. [CrossRef]
61. Zhu, Z.; Niu, H.; Liu, Z.; Liu, S. Decomposition and Reactivity of NH_4HSO_4 on V_2O_5/AC Catalysts Used for NO Reduction with Ammonia. *J. Catal.* **2000**, *195*, 268–278. [CrossRef]
62. Xu, T.; Wu, X.; Liu, X.; Cao, L.; Lin, Q.; Weng, D. Effect of barium sulfate modification on the SO_2 tolerance of V_2O_5/TiO_2 catalyst for NH_3-SCR reaction. *J. Environ. Sci.* **2017**, *57*, 110–117. [CrossRef]
63. Dong, G.-J.; Zhang, Y.-F.; Zhao, Y.; Bai, Y. Effect of the pH value of precursor solution on the catalytic performance of V_2O_5-WO_3/TiO_2 in the low temperature NH_3-SCR of NOx. *J. Fuel Chem. Technol.* **2014**, *42*, 1455–1463. [CrossRef]
64. Song, I.; Youn, S.; Lee, H.; Lee, S.G.; Cho, S.J.; Kim, D.H. Effects of microporous TiO_2 support on the catalytic and structural properties of V_2O_5/microporous TiO_2 for the selective catalytic reduction of NO by NH_3. *Appl. Catal. B Environ.* **2017**, *210*, 421–431. [CrossRef]
65. Liu, L.; Wu, X.; Ma, Y.; Zhang, X.; Ran, R.; Si, Z.; Weng, D. Potassium deactivation of Cu-SSZ-13 catalyst for NH_3-SCR: Evolution of salts, zeolite and copper species. *Chem. Eng. J.* **2019**, *383*, 123080. [CrossRef]
66. Kong, M.; Liu, Q.; Zhou, J.; Jiang, L.; Tian, Y.; Yang, J.; Ren, S.; Li, J. Effect of different potassium species on the deactivation of V_2O_5-WO_3/TiO_2 SCR catalyst: Comparison of K_2SO_4, KCl and K_2O. *Chem. Eng. J.* **2018**, *348*, 637–643. [CrossRef]
67. Orsenigo, C.; Lietti, L.; Tronconi, E.; Forzatti, P.; Bregani, F. Dynamic Investigation of the Role of the Surface Sulfates in NO_x Reduction and SO_2 Oxidation over $V_2O_5-WO_3/TiO_2$ Catalysts. *Ind. Eng. Chem. Res.* **1998**, *37*, 2350–2359. [CrossRef]
68. Liu, F.; Asakura, K.; He, H.; Shan, W.; Shi, X.; Zhang, C. Influence of sulfation on iron titanate catalyst for the selective catalytic reduction of NOx with NH_3. *Appl. Catal. B Environ.* **2011**, *103*, 369–377. [CrossRef]
69. Chen, C.; Wu, X.; Yu, W.; Gao, Y.; Weng, D.; Shi, L.; Geng, C. Potassium poisoning of titania supported deNOx catalysts: Preservation of vanadia and sacrifice of tungsten oxide. *Chin. J. Catal.* **2015**, *36*, 1287–1294. [CrossRef]
70. Dunn, J.P.; Koppula, P.R.; Stenger, H.G.; Wachs, I.E. Oxidation of sulfur dioxide to sulfur trioxide over supported vanadia catalysts. *Appl. Catal. B Environ.* **1998**, *19*, 103–117. [CrossRef]